Chemical Science

ROYAL SOCIETY OF CHEMISTRY

EDGE ARTICLE

View Article Online
View Journal | View Issue

Cite this: *Chem. Sci.*, 2025, **16**, 9348

All publication charges for this article have been paid for by the Royal Society of Chemistry

On-surface synthesis of organometallic nanorings linked by unconventional intermediates of the Ullmann reaction†

Xiaoyang Zhao, ‡[a] Liqian Liu,‡[a] Zhipeng Zhang,[a] Tianchen Qin,[b] Jun Hu,[b] Lei Ying, [a] Junfa Zhu, [b] Tao Wang *[c] and Xinrui Miao *[a]

Received 18th February 2025
Accepted 20th April 2025

DOI: 10.1039/d5sc01269d

rsc.li/chemical-science

Ullmann coupling has been one of the most important organic reactions for the formation of an aryl–aryl bond, which is of great significance in medicinal chemistry, natural product synthesis, and optoelectronic material fabrication. However, the associated reaction mechanism has not been determined with certainty and has mostly relied on theoretical calculations, since the identification of reaction intermediates lacked experimental evidence. Herein, we report the visualization of an unprecedented C–Cu–Br–Cu–C bonded intermediate state of Ullmann coupling by means of on-surface synthesis. These intermediates tend to form nanorings on a Cu(111) surface, as thermodynamically stable structures. Advanced techniques, including scanning tunneling microscopy, non-contact atomic force microscopy, and synchrotron radiation photoemission spectroscopy, together with density functional theory calculations, were used to scrutinize the structural assignments and intermediate transition process at the sub-molecular level. The C–Cu–Br–Cu–C structure is confirmed to be the precursor state of the conventional C–Cu–C intermediate during an on-surface Ullmann reaction, since their coexistence and transformation were observed experimentally. Our findings offer insights into revisiting and understanding the reaction mechanism of Ullmann coupling.

Introduction

Ullmann coupling has been intensely utilized to synthesize symmetric and asymmetric biphenyl compounds, and has a wide range of applications in medicinal chemistry, materials science, and organic synthesis.[1,2] Although high reaction efficiency and selectivity have been achieved in the past few decades, the reaction mechanism of Ullmann coupling remains elusive because the capture and accurate characterization of the reaction intermediates are challenging. Consequently, the interpretation of the reaction mechanisms of Ullmann coupling have largely relied on theoretical calculations. As for classical metal (M)-catalyzed Ullmann reaction systems, two representative mechanisms rationalized by calculations are the single electron transfer mechanism and the M(I)–M(III) ionic mechanism.[3] The latter involves a more complex pathway and has been more popular (Scheme 1a), in which an M(III) species acts as an important intermediate prior to the final formation of a C–C covalent bond (red dashed box).[4–6] However, although this predicted mechanism could be reasonable for Cu-catalyzed Ullmann coupling (Scheme 1a), it is probably not universal and has been debated because it is not possible to use it to interpret the reaction mechanism of Pd- or Ni-catalyzed Ullmann coupling.[7,8] Pd(III) and Ni(III) species are not in their common valence states; thus different reaction mechanisms in Pd- or Ni-catalyzed reaction systems need to be proposed. Therefore, an inadequate understanding of the reaction mechanism to date has been a major obstacle to the rational design of catalysts and the further development of Ullmann coupling. The key to depicting the reaction mechanism of Ullmann coupling is the effective detection and precise characterization of reaction intermediates.

The recently developed on-surface synthesis has provided an unprecedented opportunity for the visualization of reaction intermediates and products at the single-molecule level, with the aid of scanning tunneling microscopy (STM) and non-contact atomic force microscopy (nc-AFM) imaging under ultra-high vacuum conditions.[9–13] In addition, the molecule–substrate interaction helps the stabilization and thereby the capture of metastable intermediates.[14,15] With an on-surface synthesis approach, the mechanisms of several organic reactions have been unraveled at the sub-molecular scale in real

[a]*State Key Laboratory of Luminescent Materials and Devices, College of Materials Science and Engineering, South China University of Technology, Guangzhou, 510640, P. R. China. E-mail: msxrmiao@scut.edu.cn*

[b]*National Synchrotron Radiation Laboratory, University of Science and Technology of China, Hefei, 230029, P. R. China*

[c]*State Key Laboratory of Organometallic Chemistry, Shanghai Institute of Organic Chemistry, Chinese Academy of Sciences, Shanghai, 200032, P. R. China. E-mail: taowang@sioc.ac.cn*

† Electronic supplementary information (ESI) available. See DOI: https://doi.org/10.1039/d5sc01269d

‡ These authors contributed equally.

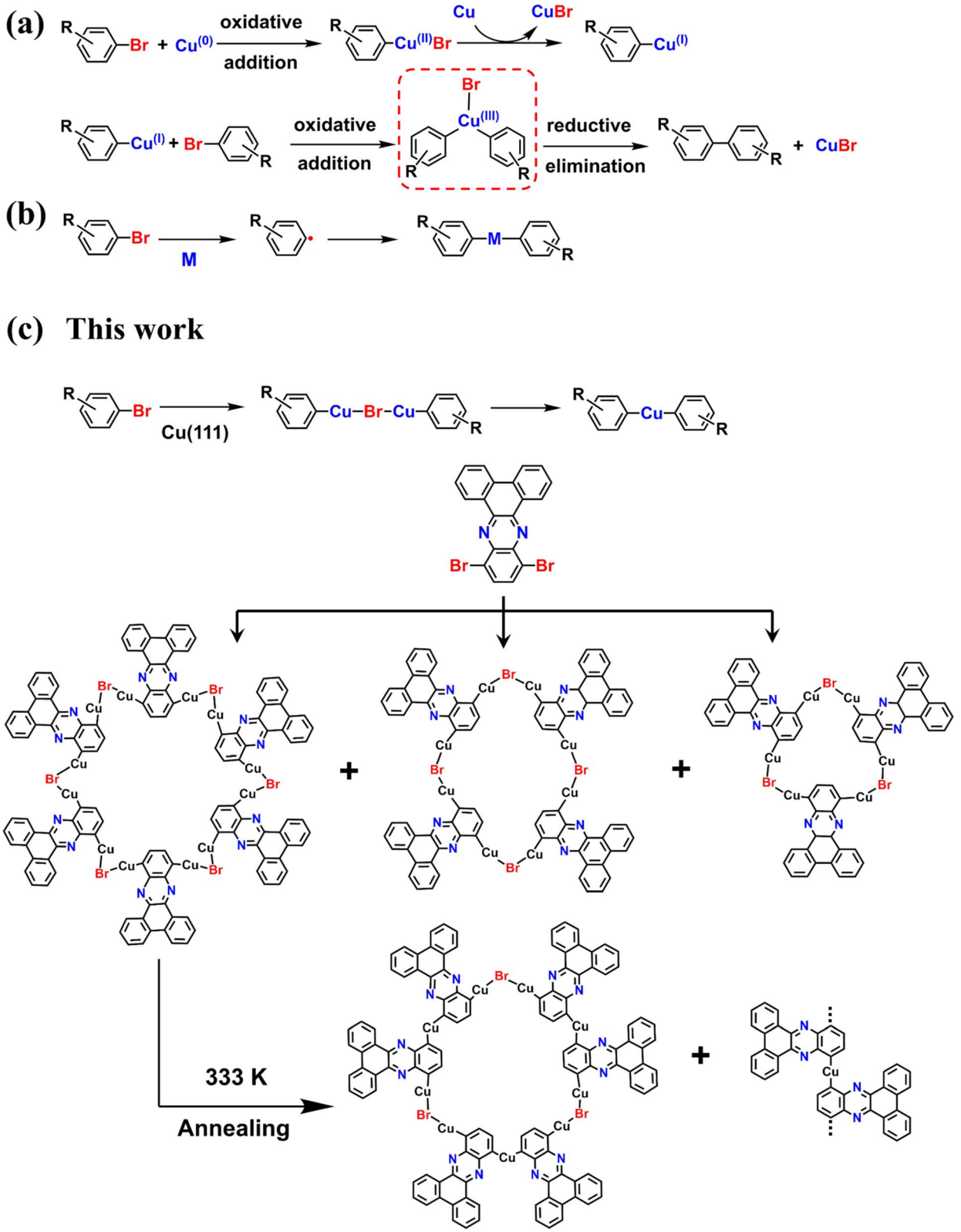

Scheme 1 Schematic illustration of Ullmann coupling reactions. (a) Possible mechanism of Cu-catalyzed Ullmann coupling in-solution chemistry. (b) The conventional reaction pathway of on-surface Ullmann coupling. (c) Reaction pathway of DBP-Br precursor on Cu(111), in which C–Cu–Br–Cu–C bonded nanorings are formed at RT and transform into C–Cu–C bonded nanorings and *trans*-dimer after annealing at 333 K.

space, such as intermolecular radical transfer,[16] ethylene polymerization,[17] and nucleation–elongation of boroxine polymer.[18–22] However, as the most widely utilized on-surface reaction for the synthesis of graphene nanoribbons and covalent networks,[23–26] the detailed reaction pathway of on-surface Ullmann coupling has been largely unknown.[27] The only conventionally captured and characterized intermediate is the C–M–C species (M = Au, Ag, Cu; Scheme 1b),[28–30] which transforms into the C–C covalent bond upon further activation. The process starting from C–X (X = Cl, Br, I) dissociation to the formation of C–M–C species is, however, unclear.[31,32] This can probably be attributed to the short lifetime of the associated C–M–X or similar intermediates, *i.e.* a negligible energy barrier from C–M–X to C–M–C species.

Note that in solution-phase Ullmann coupling, the introduction of N-containing ligands enables the coupling reaction to proceed under mild conditions.[33–35] Therefore, the N-containing ligands may influence the formation, evolution, and lifetime of intermediates, potentially contributing to the capture of intermediates. Inspired by this, herein, we investigated the reaction mechanism of N-doped brominated molecules on a Cu(111) surface by monitoring the formation of organometallic intermediates. 10,13-Dibromodibenzo[*a*,*c*]phenazine (DBP-Br) with the phenazine unit close to the brominated benzene ring was used as the precursor. Interestingly, a series of N-doped nanorings were fabricated by depositing DBP-Br on Cu(111) at room temperature (RT) (Scheme 1c), which are stabilized by unusual C–Cu–Br–Cu–C bonds, as confirmed by combined STM, nc-AFM, synchrotron radiation photoemission spectroscopy (SRPES), and density functional theory (DFT) calculations. The C–Cu–Br–Cu–C species are transformed to the conventional C–Cu–C bond upon further annealing, indicating that the former is a precursor state of the latter. Notably, the C–Cu–Br–Cu–C bonded intermediate is similar to but different from the theoretically possible counterpart in a solution-phase Ullmann reaction (red dashed box in Scheme 1a), which may arouse scientists' interests in revisiting reaction mechanism of solution-phase Ullmann coupling. This work extends insights into the Ullmann coupling mechanism by visualizing diverse reaction intermediates in real space.

Results and discussion

After depositing DBP-Br molecules with approximately 0.5 monolayer (ML) onto the Cu(111) surface kept at RT, prevailing nanorings were unexpectedly observed (Fig. 1a). 6-Membered rings are the major products, and a small amount of 4-membered nanorings (blue circles in Fig. 1a; high-resolution images can be seen in Fig. S1†) coexist. The zoom-in STM images displayed in Fig. 1b and c reveal the detailed structure of a 6-membered ring composed of six DBP units, in which the "serrations" correspond to the phenanthrene backbones and the quinoxaline groups manifest as dark "grooves" (Fig. S1†). We observed that the distance (~7.6 Å) (Fig. 1c) between adjacent DBP units is remarkably longer than that of the conventional C–Cu–C bond (~3.8 Å)[36,37] formed after the dissociation of C–Br bonds on Cu(111) at RT. Two dots are resolved in this bond; thus a direct intuition is that the bond might be a C–Cu–Cu–C motif. However, the C–Cu–Cu–C motif is extremely unstable according to DFT calculations, and is automatically

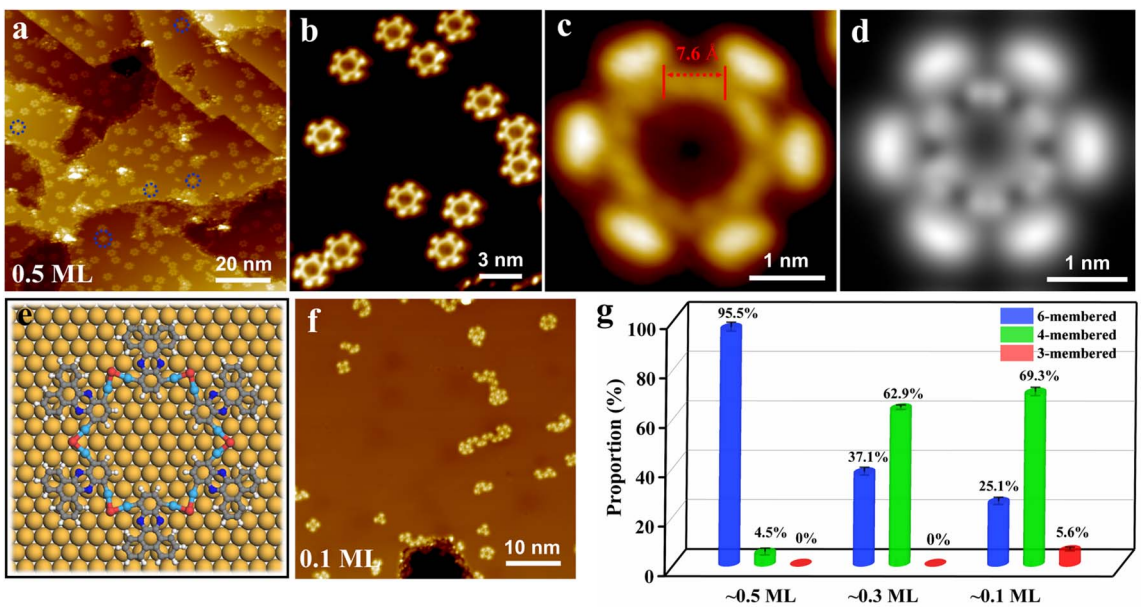

Fig. 1 Characterization of C–Cu–Br–Cu–C bonded nanorings by scanning probe microscopies. (a) Large-scale STM image recorded after depositing DBP-Br with a coverage of 0.5 ML on Cu(111) held at 300 K. (b) Typical STM image showing uniform 6-membered nanorings. (c) Close-up STM image of a single 6-membered nanoring. (d) Simulated STM image of the 6-membered nanoring using a bias voltage of 500 mV. (e) DFT-optimized molecular model of the 6-membered nanoring linked by C–Cu–Br–Cu–C bonds on the Cu(111) surface. (f) Large-scale STM image recorded after depositing DBP-Br with a coverage of 0.1 ML on Cu(111) held at 300 K. (g) Statistical analysis of the observed nanorings with different coverages on Cu(111), by counting more than 650 organometallic nanoring structures on each sample. Scanning parameters: (a–c and f) V_{bias} = 500 mV, I_{set} = 50 pA.

dissociated during optimization. Inspired by the C–Cu–Br linked intermediates in solution-phase Ullmann coupling,[33,35] we propose that the bond here may be assigned to a C–Cu–Br–Cu–C motif, as supported by the good agreement between the DFT-simulated STM image/molecular adsorption model and the corresponding experimental results (Fig. 1d, e and S1†). According to the calculation, the angle of the Cu–Br–Cu bond is about 88°, and the Br atoms are invisible within the typical range of scanning bias voltage because of their low density of electronic states. Notably, only six Br atoms are required for the formation of a C–Cu–Br–Cu–C linked six-membered nanoring, implying that other six Br atoms provided by the precursors should adsorb on the Cu(111) surface, which are clearly visible in some high-resolution STM images (Fig. S2†).[38,39]

The above organometallic nanorings are linked through a novel C–Cu–Br–Cu–C bond, extending the family of functional organic nanorings. Interestingly, the topology of these nanorings can be tuned by molecular coverage. As shown in Fig. 1f and S3–S5,† the dominant nanoring products on Cu(111) at RT evolved from the larger 6-membered ring, to smaller 4- and 3-membered rings, as the coverage decreased. In particular, the smallest 3-membered ring,[40] which is difficult to synthesize on surfaces, starts to be generated only at an extremely low coverage of 0.1 M L.[36] These nanorings kept their structural integrity even when the sample was left at RT for four days (Fig. S6†), exhibiting high thermostability.

To investigate intermediate evolution from the unusual C–Cu–Br–Cu–C motif to the conventional C–Cu–C motif of Ullmann coupling on Cu(111), the sample was annealed at 333 K for 20 min. As shown in the representative STM images (Fig. 2a, S7 and S8†), the majority of 6-membered nanorings opened and the morphology of the surviving nanorings had changed compared to the original ones in Fig. 1. An example of such 6-membered nanorings is displayed in Fig. 2b and c. While three bonds kept their original configuration as the C–Cu–Br–Cu–C connection, the other three bonds became much shorter and their length was measured to be about 3.8 Å. This strongly implies that the short bonds are assigned to the conventional C–Cu–C bonds in Ullmann coupling on Cu(111), where the bright dots correspond to the Cu adatoms.[30] In addition, the majority of the observed *trans*-dimer and chain-like structure formed after ring-opening are also linked by C–Cu–C bonds, as represented by the STM image of a *trans*-dimer in Fig. 2d. The chemical structure matches well with the corresponding STM image (Fig. 2e), in which the bright dot is again assigned to an Cu adatom and the phenyls binding to Cu show relatively dark contrast because of their low adsorption height (Fig. S9†). Such a transformation described above provides direct evidence that the unusual C–Cu–Br–Cu–C intermediate starts evolving into the C–Cu–C motif under these conditions. In this process, the nanorings tend to open in order to avoid large ring tension; note that the formed C–Cu–C bond (the angle is typically >160°)[41–43]

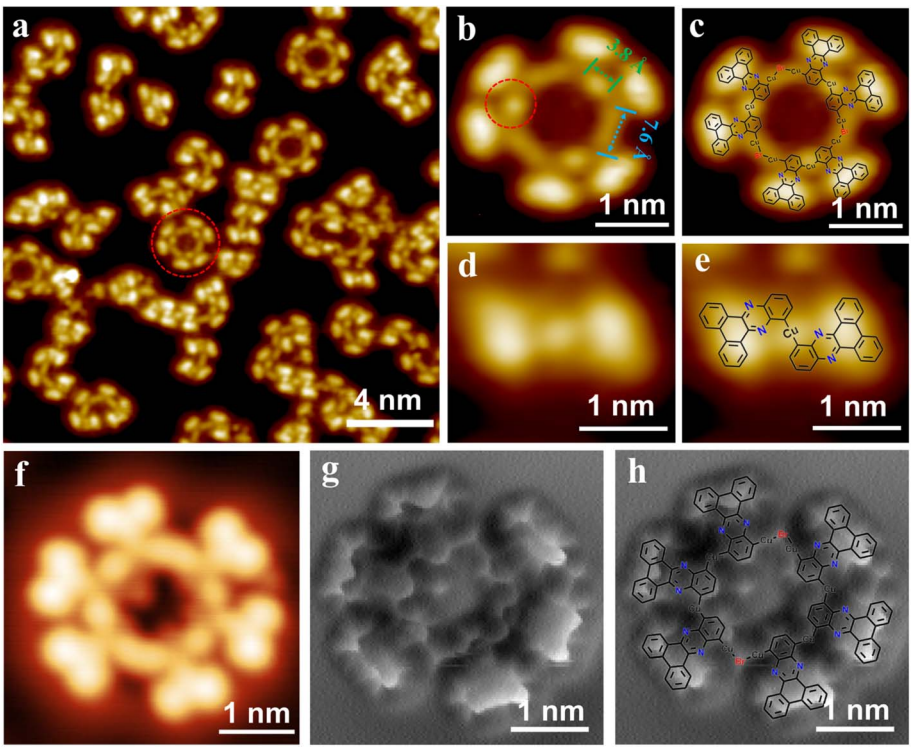

Fig. 2 Transformation from C–Cu–Br–Cu–C to C–Cu–C bonded intermediates and bond-resolving image of C–Cu–Br–Cu–C bonded nanoring. (a) Overview STM image revealing the structural evolution by annealing the sample at 333 K. (b) Zoom-in STM image of a 6-membered ring containing both C–Cu–Br–Cu–C and C–Cu–C bonds. The corresponding chemical structure is overlapped in (c). (d) Zoom-in STM image of a *trans*-dimer. The corresponding chemical structure is overlapped in (e). (f) Representative STM image and (g) nc-AFM image of a 6-membered ring containing both C–Cu–Br–Cu–C and C–Cu–C bonds. The corresponding chemical structure is overlapped in (h). Scanning parameters: (a–c and f) $V_{bias} = 500$ mV, $I_{set} = 50$ pA.

cannot possibly be bent at a similar angle to that of the Cu–Br–Cu bond (80–90°; Fig. S10†) to retain the prefect cyclic geometry.

To further confirm the structure of organometallic intermediates linked by C–Cu–Br–Cu–C and C–Cu–C bonds, a bond-resolving (BR) nc-AFM experiment was performed using a CO-functionalized probe.[44] A 6-membered nanoring containing two C–Cu–C and four C–Cu–Br–Cu–C bonds is shown in Fig. 2f and g. According to the BR nc-AFM image, the C–Cu–C bond manifests as a uniform and continuous line, and the Br atom presents as a bright protrusion in the BR nc-AFM image, in excellent agreement with previous reports.[38,45–47] In addition, the structural model optimized by DFT calculations matches well with the corresponding nc-AFM image (Fig. 2h). We note that, similar to the case in Fig. 2d, the pyridine moiety and the central phenyl appear darker than the phenanthrene backbone because they bend to the Cu(111) surface, driven by the strong interaction between the pyridine moiety and the substrate (Fig. S9†).

On the basis of the coexistence during annealing-stimulated transformation of C–Cu–Br–Cu–C and C–Cu–C bonded organometallic intermediates, we confirm that the unusual C–Cu–Br–Cu–C motif is the precursor state of a C–Cu–C bond, thus filling in the blank in the mechanism between C–X dissociation and C–Cu–C generation in an on-surface Ullmann coupling reaction. Interestingly, a few nanorings containing Cu–Br–Cu bonds with a smaller angle where Br is further away from the ring center were occasionally observed experimentally (Fig. S11†). In this case, the Br atom is leaving the nanoring but is still grasped by the Cu coordination interaction, which might be a metastable transition or intermediate states of the transformation process between C–Cu–Br–Cu–C and C–Cu–C motifs.

The C–Cu–Br–Cu–C species completely transformed into the C–Cu–C linked chain at 353 K, in which monomer units align in a *trans*-configuration (Fig. S12†). This is opposite to the case of C–Cu–Br–Cu–C linked nanorings, where the neighboring monomers are connected with a *cis*-configuration. We calculated the energy of both *trans*- and *cis*-structures of C–Cu–Br–Cu–C/C–Cu–C organometallic species on Cu(111) and confirmed that a *cis*-configuration is energetically more favorable for the C–Cu–Br–Cu–C bonded intermediate while a *trans*-configuration is energetically more favorable for the C–Cu–C bonded intermediate (Fig. S13†), in good agreement with experiment. Further annealing at a higher temperature of 413 K resulted in the dissociation of C–Cu–C bonds, but C–C covalent bonds were only occasionally observed due to the strong steric hindrance (Fig. S14†). The dominant products are debrominated monomers and they aggregate through Br···H hydrogen bonding (Fig. S15†).[39]

The whole reaction process and further product confirmation in each reaction step were monitored by synchrotron radiation photoemission spectroscopy (SRPES) experiments. As shown in Fig. 3a, by fitting the original experimental data, four C species were identified at different temperatures. Based on the electronegativity of atoms linking the carbon and according to numerous previous studies,[48–50] the order of binding energy (BE) of C 1s should be C[C_2N] (285.5 eV) > C[C_3]&C[C_2CuBr] (285.0 eV) > C[C_2H] (284.4 eV) > C[C_2Cu] (283.9 eV), as represented by red, green, blue, and purple lines, respectively (Fig. 3a). We note that because a Br atom is a strong electron-withdrawing group, which significantly attracts the electron of a Cu atom, electron donation from Cu to C is suppressed (Fig. S16†). Therefore, the BE of C[C_2CuBr] is close to that of C[C_3]. We thus consider the two types of carbons as the same component in the spectral fitting. At RT, the ratio of C[C_2N] : C[C_3]&C[C_2CuBr] : C[C_2H] = 0.35 : 0.6 : 1 obtained from the experimental results, is very close to the ideal value derived from the chemical model of a C–Cu–Br–Cu–C bonded nanoring (Fig. 3b). Importantly, this experimental fact provides strong

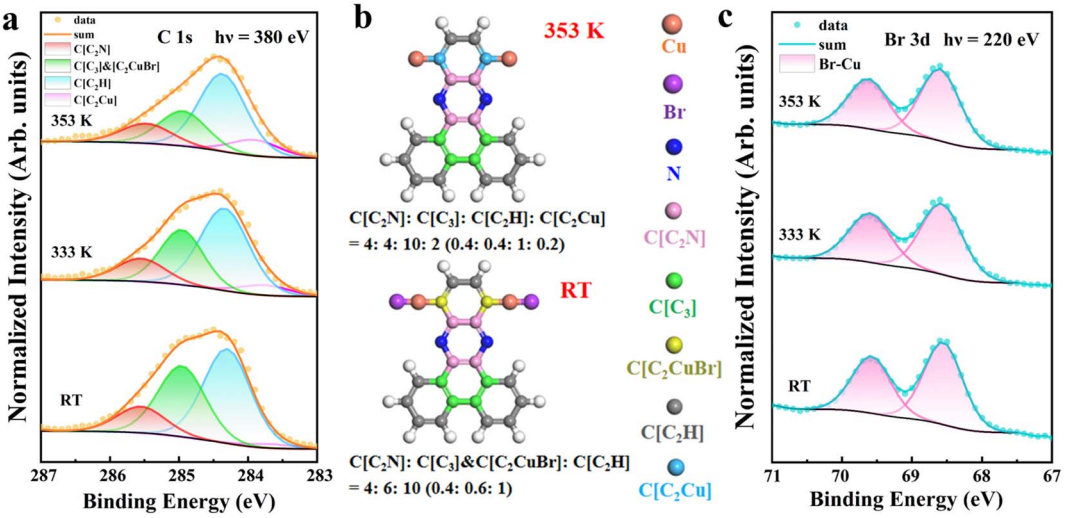

Fig. 3 SRPE spectra C 1s and of Br 3d showing the structural evolution of DBP-Br on the Cu(111) surface. (a) C 1s SRPE spectra of DBP-Br on Cu(111) recorded by annealing the sample at different temperatures. Circles represent original experimental data and solid lines represent the fitting. (b) Structural models of respective major products at RT and 353 K. Different atoms are depicted by different colors to illustrate their chemical environments. The ideal ratios of different C atoms as derived from the chemical structures are shown below. (c) Br 3d SRPE spectra of DBP-Br on Cu(111) recorded by annealing the sample at different temperatures.

evidence for the structural assignment of C–Cu–Br–Cu–C, because the formation of other possible structures linked by C–$(Cu)_n$–C (n = 2, 3) should give rise to the appearance of a C [C_2Cu] signal at a low BE,[49,51] which is absent in our experiments. Annealing at 333 K leads to the appearance of the signal of C[C_2Cu] in C 1s and a decrease in intensity of C[C_2CuBr], indicating that the transformation from C–Cu–Br–Cu–C to C–Cu–C was activated at this temperature, also in good agreement with STM observations. The ratio of the four components changed to C[C_2N] : C[C_3]&[C_2CuBr] : C[C_2H] : C[C_2Cu] = 0.36 : 0.4 : 1:0.2 upon further annealing at 353 K, matching well with the ideal stoichiometric value of the C–Cu–C linked product (0.4 : 0.4 : 1 : 0.2). This in turn indicates a complete transformation from C–Cu–Br–Cu–C to C–Cu–C intermediates at 353 K, further supporting the associated STM results.

On the other hand, only one kind of Br species was identified in the Br 3d spectra (Fig. 3c), featuring a spin–orbit doublet Br $3d_{3/2}$ and $3d_{5/2}$ with BE of 69.7 and 68.6 eV, respectively.[52–54] This is because Br adatoms on Cu(111) generated by C–Br and C–Cu–Br–Cu–C dissociation have a similar chemical environment to the Br atoms in a C–Cu–Br–Cu–C bond. In both cases, Cu atoms interact with and donate electrons to the linked Br atoms, although one kind of Cu is generated from the Cu(111) surface and the other corresponds to the Cu adatom trapped by the molecules.

To elucidate an atomistic understanding of the transformation process from C–Cu–Br–Cu–C to C–Cu–C bonds on the Cu(111) surface, we utilized climbing images nudged elastic band (CI-NEB) to calculate the reaction pathway.[55,56] To balance the computational cost and accuracy, the structure of the DBP unit is represented by a quinoxaline unit. The reaction path barrier diagram calculated with DFT is shown in Fig. 4. The initial reaction state (IS) shows that two quinoxaline units adsorbed on Cu(111) are connected by the C–Cu–Br–Cu–C bond. In the next step, one Br atom leaves the C–Cu–Br–Cu–C bond, by going across a reasonable energy barrier (1.47 eV; TS1) to the intermediate state (0.61 eV; Int). Further, one Cu atom on one quinoxaline unit gradually leaves, and the quinoxaline unit moves toward another quinoxaline unit to form a more stable C–Cu–C bonded structure (−0.54 eV; FS), crossing a relatively low energy barrier (0.76 eV; TS2). The whole reaction undergoes an exothermic path, indicating that the transition from C–Cu–Br–Cu–C to C–Cu–C bonds is irreversible.

To our knowledge, such C–Cu–Br–Cu–C organometallic intermediates have not been reported in on-surface synthesis. Although the introduction of N atoms into the precursor molecule might be an indispensable factor for the formation of C–Cu–Br–Cu–C intermediates, it is not the only decisive parameter, because such an intermediate has never been observed *via* the on-surface synthesis of other N-doped aryl halides.[57–59] Therefore, we propose that the relative position of N atoms together with the special molecular backbone, as well as the formation of thermodynamically stable nanorings[60,61] may also induce the generation of C–Cu–Br–Cu–C organometallic intermediates, by improving the stability and elongating the lifetime of C–Cu–Br–Cu–C intermediates. Note that the former determines the molecular adsorption geometry and steric hindrance effect, which is closely related to the substrate–molecule interaction and charge transfer (Fig. S16†),[62–66] thus associating with the formation barrier and structural stability of the C–Cu–Br–Cu–C intermediates. In addition, previous studies reported that C–Cu–C has been formed at RT,[67,68] whereas in

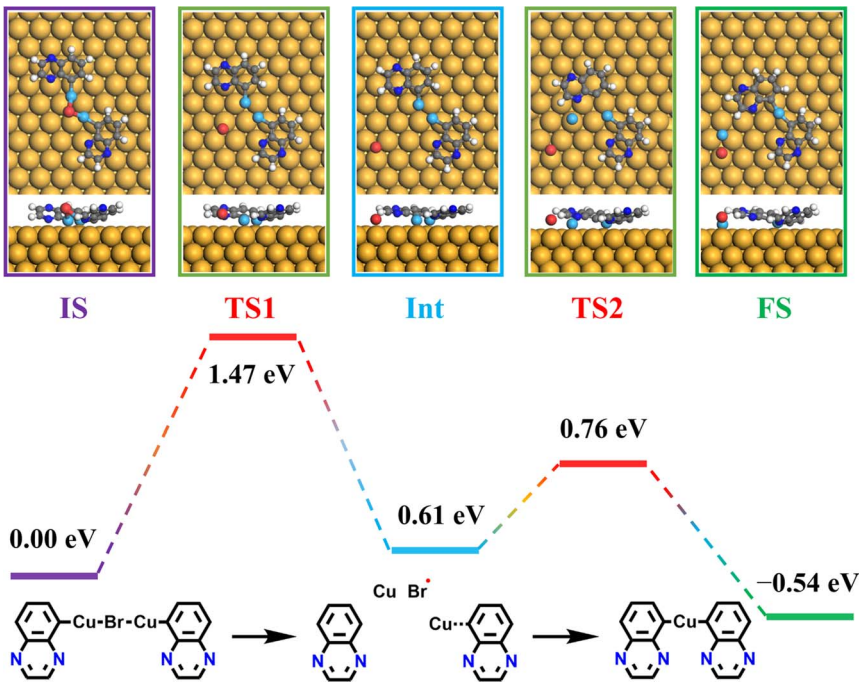

Fig. 4 DFT calculated structural transformation from C–Cu–Br–Cu–C to C–Cu–C bonded intermediates on Cu(111). The reaction pathway and energy profile in each step are presented.

this work, a C–Cu–Br–Cu–C linked ring structure is observed at RT, implying that the formation of the nanorings provides further stability to the system. Further studies will focus on how the precursor structure influences the formation of the C–Cu–Br–Cu–C bonded intermediates by tuning parameters, including the position of nitrogen substitution, length and shape of the molecular backbone, amount of charge transfer (as determined by ionization energy),[63] and ring tension, by designing more structurally similar precursors.

Conclusions

We report an unusual C–Cu–Br–Cu–C bonded intermediate in an Ullmann coupling reaction of DBP-Br on Cu(111), forming high-yield N-doped nanorings. The topology of the nanorings can be well tuned by changing the coverage of precursors on the surface. By careful inspection of structural transformation upon sample annealing, the C–Cu–Br–Cu–C motif is confirmed to be the precursor state of the conventional C–Cu–C intermediate in on-surface Ullmann coupling. Structural validation is offered by the combination of STM, nc-AFM, SRPES, and DFT calculations. We propose that the formation of C–Cu–Br–Cu–C bonded nanorings is attributed to the synergy of multiple factors, including molecular adsorption geometry, molecule–substrate interaction, and charger transfer, as well as the stabilizing effect of the nanoring. These factors together contribute to a longer lifetime of the otherwise unstable C–Cu–Br–Cu–C intermediate. The visualization of an intermediate between C–X dissociation and C–Cu–C formation in this work extends the diversity of organometallic intermediates of Ullmann coupling on metal surfaces. Notably, the C–Cu–Br–Cu–C intermediate is similar to the Cu(III) species proposed in solution-phase Ullmann coupling (Scheme 1c). However, in the C–Cu–Br–Cu–C intermediate reported in this work, Cu holds a valence state between +1 and +2, different from the +3 of the similar Cu(III) intermediate in the Cu(I)–Cu(III) ionic mechanism in solution. Therefore, the mechanism rationalized in this work may also reasonably interpret the reaction pathway in Ni- or Pd-catalyzed Ullmann coupling reactions in addition to Cu-catalyzed systems in solution, since the associated intermediates hold the most common valence state (+1 or +2) of Ni and Pd. We thus propose a possibility that the C–M–Br–M–C intermediate might exist in conventional solution-phase metal-catalyzed Ullmann couplings, although the detailed mechanism is likely to be different from that on the surface. This work opens up a new avenue for revisiting the reaction mechanisms of Ullmann coupling both on the surface and in solution.

Data availability

Experimental details and additional results can be found in the ESI.† All other data will be available on request.

Author contributions

X. M. conceived the project and designed the experiments. X. Z., L. L. and Z. Z. conducted the STM experiments under the supervision of T. W. and X. M. X. Z. performed theoretical studies. X. Z., T. Q. and J. H. performed SRPES experiments under the supervision of J. Z. T. W. and L. L. carried out the nc-AFM experiments. L. Y. synthesized precursor molecules. X. Z., L. L., Z. Z., T. W. and X. M. interpreted the results. X. Z., X. M., and T. W. co-wrote the manuscript with suggestions from all authors. All the authors discussed the results and commented on the manuscript.

Conflicts of interest

There are no conflicts to declare.

Acknowledgements

Financial support from the National Natural Science Foundation of China (22172055), the Strategic Priority Research Program of the Chinese Academy of Sciences (XDB1180000), the Science Fund for Distinguished Young Scholars of Guangdong Province (2023B1515040026), and the Natural Science Foundation of Guangdong Province (2022A1515011892). The authors thank Dr Bingkai Yuan for nc-AFM characterization at the Vacuum Interconnected Nanotech Workstation (Nano-X), Suzhou Institute of Nano-Tech and Prof. Chao Zheng at Shanghai Institute of Organic Chemistry, CAS, for insightful discussions.

References

1 C. P. Delaney, E. Lin, Q. Huang, I. F. Yu, G. Rao, L. Tao, A. Jed, S. M. Fantasia, K. A. Püntener, R. D. Britt and J. F. Hartwig, *Science*, 2023, **381**, 1079–1085.
2 J. Feng, L.-L. Xi, C.-J. Lu and R.-R. Liu, *Chem. Soc. Rev.*, 2024, **53**, 9560–9581.
3 L. Kurti and B. Czako, *Strategic applications of named reactions in organic synthesis*, Elsevier, 2005.
4 R. Akhtar, A. F. Zahoor, M. Irfan, T. H. Bokhari and A. ul Haq, *Chem. Pap.*, 2022, **76**, 7275–7293.
5 C. Sharma, A. K. Srivastava, D. Sharma and R. K. Joshi, *Org. Chem. Front.*, 2022, **9**, 6252–6258.
6 O. Vyhivskyi, D. N. Laikov, A. V. Finko, D. A. Skvortsov, I. V. Zhirkina, V. A. Tafeenko, N. V. Zyk, A. G. Majouga and E. K. Beloglazkina, *J. Org. Chem.*, 2020, **85**, 3160–3173.
7 F. Khan, M. Dlugosch, X. Liu and M. G. Banwell, *Acc. Chem. Res.*, 2018, **51**, 1784–1795.
8 B. Zhu, L.-K. Yan, L.-S. Yao, H. Ren, R.-H. Li, W. Guan and Z.-M. Su, *Chem. Commun.*, 2018, **54**, 7959–7962.
9 S. Clair and D. G. de Oteyza, *Chem. Rev.*, 2019, **119**, 4717–4776.
10 N. Pavliček, B. Schuler, S. Collazos, N. Moll, D. Pérez, E. Guitián, G. Meyer, D. Peña and L. Gross, *Nat. Chem.*, 2015, **7**, 623–628.
11 Q. Zhong, A. Ihle, S. Ahles, H. A. Wegner, A. Schirmeisen and D. Ebeling, *Nat. Chem.*, 2021, **13**, 1133–1139.
12 D. G. de Oteyza, P. Gorman, Y.-C. Chen, S. Wickenburg, A. Riss, D. J. Mowbray, G. Etkin, Z. Pedramrazi, H.-Z. Tsai, A. Rubio, M. F. Crommie and F. R. Fischer, *Science*, 2013, **340**, 1434–1437.

13 M. Di Giovannantonio, M. El Garah, J. Lipton-Duffin, V. Meunier, L. Cardenas, Y. Fagot Revurat, A. Cossaro, A. Verdini, D. F. Perepichka, F. Rosei and G. Contini, *ACS Nano*, 2013, **7**, 8190–8198.
14 B. Qie, Z. Wang, J. Jiang, Z. Zhang, P. H. Jacobse, J. Lu, X. Li, F. Liu, A. N. Alexandrova, S. G. Louie, M. F. Crommie and F. R. Fischer, *Science*, 2024, **384**, 895–901.
15 Z. Zeng, D. Guo, T. Wang, Q. Chen, A. Matěj, J. Huang, D. Han, Q. Xu, A. Zhao, P. Jelínek, D. G. de Oteyza, J.-S. McEwen and J. Zhu, *J. Am. Chem. Soc.*, 2022, **144**, 723–732.
16 J. Wang, K. Niu, H. Zhu, C. Xu, C. Deng, W. Zhao, P. Huang, H. Lin, D. Li, J. Rosen, P. Liu, F. Allegretti, J. V. Barth, B. Yang, J. Björk, Q. Li and L. Chi, *Nat. Commun.*, 2024, **15**, 3030.
17 W. Guo, J. Yin, Z. Xu, W. Li, Z. Peng, C. J. Weststrate, X. Yu, Y. He, Z. Cao, X. Wen, Y. Yang, K. Wu, Y. Li, J. W. Niemantsverdriet and X. Zhou, *Science*, 2022, **375**, 1188–1191.
18 G. Zhan, Z.-F. Cai, K. Strutyński, L. Yu, N. Herrmann, M. Martínez-Abadía, M. Melle-Franco, A. Mateo-Alonso and S. D. Feyter, *Nature*, 2022, **603**, 835–840.
19 D. Dettmann, M. Panighel, N. Preetha Genesh, G. Galeotti, O. MacLean, M. Farnesi Camellone, T. K. Johal, S. Fabris, C. Africh, D. F. Perepichka, F. Rosei and G. Contini, *J. Am. Chem. Soc.*, 2024, **146**, 24493–24502.
20 A. Kinikar, M. Di Giovannantonio, J. I. Urgel, K. Eimre, Z. Qiu, Y. Gu, E. Jin, A. Narita, X.-Y. Wang, K. Müllen, P. Ruffieux, C. A. Pignedoli and R. Fasel, *Nat. Synth.*, 2022, **1**, 289–296.
21 T. Wang and J. Zhu, *Surf. Sci. Rep.*, 2019, **74**, 97–140.
22 Z.-Y. Yi, Z.-C. Wang, R.-N. Li, Z.-H. Li, J.-J. Duan, X.-Q. Yang, Y.-Q. Wang, T. Chen, D. Wang and L.-J. Wan, *J. Am. Chem. Soc.*, 2024, **146**, 11342–11351.
23 C. Steiner, J. Gebhardt, M. Ammon, Z. Yang, A. Heidenreich, N. Hammer, A. Görling, M. Kivala and S. Maier, *Nat. Commun.*, 2017, **8**, 14765.
24 G. Galeotti, F. De Marchi, E. Hamzehpoor, O. MacLean, M. Rajeswara Rao, Y. Chen, L. V. Besteiro, D. Dettmann, L. Ferrari, F. Frezza, P. M. Sheverdyaeva, R. Liu, A. K. Kundu, P. Moras, M. Ebrahimi, M. C. Gallagher, F. Rosei, D. F. Perepichka and G. Contini, *Nat. Mater.*, 2020, **19**, 874–880.
25 J. Cai, P. Ruffieux, R. Jaafar, M. Bieri, T. Braun, S. Blankenburg, M. Muoth, A. P. Seitsonen, M. Saleh, X. Feng, K. Müllen and R. Fasel, *Nature*, 2010, **466**, 470–473.
26 L. Dong, P. N. Liu and N. Lin, *Acc. Chem. Res.*, 2015, **48**, 2765–2774.
27 M. Fritton, D. A. Duncan, P. S. Deimel, A. Rastgoo-Lahrood, F. Allegretti, J. V. Barth, W. M. Heckl, J. Björk and M. Lackinger, *J. Am. Chem. Soc.*, 2019, **141**, 4824–4832.
28 Q. Fan, L. Liu, J. Dai, T. Wang, H. Ju, J. Zhao, J. Kuttner, G. Hilt, J. M. Gottfried and J. Zhu, *ACS Nano*, 2018, **12**, 2267–2274.
29 A. Berdonces-Layunta, F. Schulz, F. Aguilar-Galindo, J. Lawrence, M. S. G. Mohammed, M. Muntwiler, J. Lobo-Checa, P. Liljeroth and D. G. de Oteyza, *ACS Nano*, 2021, **15**, 16552–16561.
30 W. Wang, X. Shi, S. Wang, M. A. Van Hove and N. Lin, *J. Am. Chem. Soc.*, 2011, **133**, 13264–13267.
31 Q. Fan, C. Wang, L. Liu, Y. Han, J. Zhao, J. Zhu, J. Kuttner, G. Hilt and J. M. Gottfried, *J. Phys. Chem. C*, 2014, **118**, 13018–13025.
32 Q. Fan, T. Wang, L. Liu, J. Zhao, J. Zhu and J. M. Gottfried, *J. Chem. Phys.*, 2015, **142**, 101906.
33 R. Giri, A. Brusoe, K. Troshin, J. Y. Wang, M. Font and J. F. Hartwig, *J. Am. Chem. Soc.*, 2018, **140**, 793–806.
34 S. Perveen, S. Zhang, L. Wang, P. Song, Y. Ouyang, J. Jiao, X.-H. Duan and P. Li, *Angew. Chem., Int. Ed.*, 2022, **61**, e202212108.
35 Q. Yang, Y. Zhao and D. Ma, *Org. Process Res. Dev.*, 2022, **26**, 1690–1750.
36 C. K. Krug, D. Nieckarz, Q. Fan, P. Szabelski and J. M. Gottfried, *Chem. - Eur. J.*, 2020, **26**, 7647–7656.
37 F. Xiang, A. Gemeinhardt and M. A. Schneider, *ACS Nano*, 2018, **12**, 1203–1210.
38 S. Zint, D. Ebeling, T. Schlöder, S. Ahles, D. Mollenhauer, H. A. Wegner and A. Schirmeisen, *ACS Nano*, 2017, **11**, 4183–4190.
39 Y. Lin, Z. Huang, X. Wen, W. Rong, Z. Peng, M. Diao, L. Xing, J. Dai, X. Zhou and K. Wu, *ACS Nano*, 2020, **14**, 17134–17141.
40 D.-Y. Li, Y. Wang, X.-Y. Hou, Y.-T. Ren, L.-X. Kang, F.-H. Xue, Y.-C. Zhu, J.-W. Liu, M. Liu, X.-Q. Shi, X. Qiu and P.-N. Liu, *Angew. Chem., Int. Ed.*, 2022, **61**, e202117714.
41 Y.-Q. Zhang, M. Paszkiewicz, P. Du, L. Zhang, T. Lin, Z. Chen, S. Klyatskaya, M. Ruben, A. P. Seitsonen, J. V. Barth and F. Klappenberger, *Nat. Chem.*, 2018, **10**, 296–304.
42 T. Wang, Q. Fan, L. Feng, Z. Tao, J. Huang, H. Ju, Q. Xu, S. Hu and J. Zhu, *ChemPhysChem*, 2017, **18**, 3329–3333.
43 C. Fan, B. Sun, Z. Li, J. Shi, T. Lin, J. Fan and Z. Shi, *Angew. Chem., Int. Ed.*, 2021, **60**, 13896–13899.
44 L. Gross, F. Mohn, N. Moll, P. Liljeroth and G. Meyer, *Science*, 2009, **325**, 1110–1114.
45 Q. Li, B. Yang, J. Björk, Q. Zhong, H. Ju, J. Zhang, N. Cao, Z. Shi, H. Zhang, D. Ebeling, A. Schirmeisen, J. Zhu and L. Chi, *J. Am. Chem. Soc.*, 2018, **140**, 6076–6082.
46 M. Liu, S. Li, J. Zhou, Z. Zha, J. Pan, X. Li, J. Zhang, Z. Liu, Y. Li and X. Qiu, *ACS Nano*, 2018, **12**, 12612–12618.
47 M. Telychko, J. Su, A. Gallardo, Y. Gu, J. I. Mendieta-Moreno, D. Qi, A. Tadich, S. Song, P. Lyu, Z. Qiu, H. Fang, M. J. Koh, J. Wu, P. Jelínek and J. Lu, *Angew. Chem., Int. Ed.*, 2019, **58**, 18591–18597.
48 D. Han, H. Ding, J. Xiong, T. Qin, X. Cheng, J. Hu, Q. Xu and J. Zhu, *ACS Nano*, 2024, **18**, 28946–28955.
49 T. Qin, D. Guo, J. Xiong, X. Li, L. Hu, W. Yang, Z. Chen, Y. Wu, H. Ding, J. Hu, Q. Xu, T. Wang and J. Zhu, *Angew. Chem., Int. Ed.*, 2023, **62**, e202306368.
50 M. Tenorio, C. Moreno, M. Vilas-Varela, J. Castro-Esteban, P. Febrer, M. Pruneda, D. Peña and A. Mugarza, *Small Methods*, 2024, **8**, 2300768.
51 R. Gutzler, L. Cardenas, J. Lipton-Duffin, M. El Garah, L. E. Dinca, C. E. Szakacs, C. Fu, M. Gallagher,

M. Vondráček, M. Rybachuk, D. F. Perepichka and F. Rosei, *Nanoscale*, 2014, **6**, 2660–2668.
52 J. Hu, Z. Liang, H. Wang, H. Zhang, C. Huang, L. Xie, Z. Li, Z. Jiang, H. Huang and F. Song, *Appl. Surf. Sci.*, 2021, **566**, 150663.
53 D. Peyrot, M. G. Silly and F. Silly, *J. Phys. Chem. C*, 2017, **121**, 26815–26821.
54 H. Wang, Y. Wang, C. Zheng, P. Wang, Z. Hu and H.-Y. Gao, *J. Phys. Chem. Lett.*, 2024, **15**, 10535–10543.
55 J. Björk, *J. Phys.: Condens. Matter*, 2016, **28**, 083002.
56 G. Henkelman, B. P. Uberuaga and H. Jónsson, *J. Chem. Phys.*, 2000, **113**, 9901–9904.
57 L. Grill and S. Hecht, *Nat. Chem.*, 2020, **12**, 115–130.
58 H. Jiang, J. Lu, F. Zheng, Z. Zhu, Y. Yan and Q. Sun, *Chem. Commun.*, 2023, **59**, 8067–8070.
59 J. Xu, S. Xing, J. Hu and Z. Shi, *Commun. Chem.*, 2024, **7**, 40.
60 Q. Fan, T. Wang, J. Dai, J. Kuttner, G. Hilt, J. M. Gottfried and J. Zhu, *ACS Nano*, 2017, **11**, 5070–5079.
61 C. K. Krug, Q. Fan, F. Fillsack, J. Glowatzki, N. Trebel, L. J. Heuplick, T. Koehler and J. M. Gottfried, *Chem. Commun.*, 2018, **54**, 9741–9744.
62 M. Hollerer, D. Lüftner, P. Hurdax, T. Ules, S. Soubatch, F. S. Tautz, G. Koller, P. Puschnig, M. Sterrer and M. G. Ramsey, *ACS Nano*, 2017, **11**, 6252–6260.
63 T. Wang, A. Berdonces-Layunta, N. Friedrich, M. Vilas-Varela, J. P. Calupitan, J. I. Pascual, D. Peña, D. Casanova, M. Corso and D. G. de Oteyza, *J. Am. Chem. Soc.*, 2022, **144**, 4522–4529.
64 J. Xu, X. Zhu, S. Tan, Y. Zhang, B. Li, Y. Tian, H. Shan, X. Cui, A. Zhao, Z. Dong, J. Yang, Y. Luo, B. Wang and J. G. Hou, *Science*, 2021, **371**, 818–822.
65 J. Ren, M. Koy, H. Osthues, B. S. Lammers, C. Gutheil, M. Nyenhuis, Q. Zheng, Y. Xiao, L. Huang, A. Nalop, Q. Dai, H.-J. Gao, H. Mönig, N. L. Doltsinis, H. Fuchs and F. Glorius, *Nat. Chem.*, 2023, **15**, 1737–1744.
66 G. Wang, A. Rühling, S. Amirjalayer, M. Knor, J. B. Ernst, C. Richter, H.-J. Gao, A. Timmer, H.-Y. Gao, N. L. Doltsinis, F. Glorius and H. Fuchs, *Nat. Chem.*, 2017, **9**, 152–156.
67 S. Sun, B. Li, B. Fu, Z. Ruan, H. Zhang, W. Xiong, Y. Zhang, G. Niu, J. Lu, X. Zuo, L. Gao and J. Cai, *Chin. Chem. Lett.*, 2022, **33**, 5142–5146.
68 J. P. Calupitan, T. Wang, A. Pérez Paz, B. Álvarez, A. Berdonces-Layunta, P. Angulo-Portugal, R. Castrillo-Bodero, F. Schiller, D. Peña, M. Corso, D. Pérez and D. G. de Oteyza, *J. Phys. Chem. Lett.*, 2023, **14**, 947–953.